



Fermi National Accelerator Laboratory

FERMILAB-Pub-94/376

Macroparticle Simulation for Stochastic Cooling

A. Gerasimov

*Fermi National Accelerator Laboratory
P.O. Box 500, Batavia, Illinois 60510*

November 1994

Submitted to *Particle Accelerators*

Disclaimer

This report was prepared as an account of work sponsored by an agency of the United States Government. Neither the United States Government nor any agency thereof, nor any of their employees, makes any warranty, express or implied, or assumes any legal liability or responsibility for the accuracy, completeness, or usefulness of any information, apparatus, product, or process disclosed, or represents that its use would not infringe privately owned rights. Reference herein to any specific commercial product, process, or service by trade name, trademark, manufacturer, or otherwise, does not necessarily constitute or imply its endorsement, recommendation, or favoring by the United States Government or any agency thereof. The views and opinions of authors expressed herein do not necessarily state or reflect those of the United States Government or any agency thereof.

Macroparticle simulation for stochastic cooling.

A.Gerasimov,

Fermi National Accelerator Laboratory*,
P.O.Box 500, Batavia, IL 60505, USA

December 8, 1994

Abstract

The feasibility of the macroparticle simulation of stochastic (momentum) cooling is discussed. A computationally effective algorithm for simulating the particle dynamics is proposed. The scaling laws for the number of particles and cooling system bandwidth are numerically checked. Results of simulation of the momentum stacking in a simplified model are presented, indicating that reproducing 3 orders of magnitude in the density variation is easily achievable.

1 Introduction.

The performance of the \bar{p} accumulating rings is usually simulated by numerically solving the Fokker-Planck (FP) equation for the momentum cooling /1/. This approach however can not be easily extended to account for many real-life complications, particularly the two-way transverse-longitudinal coupling due to the finite betatron size at the pickup. Indeed, the computational complexity of the Fokker-Planck solvers grows with the dimensionality of the space p as N^p (N being the number of points on the grid), so going from $p = 1$ to $p = 2$ in the situation when the code for $p = 1$ case is already quite slow /2/, would most likely be not feasible. An alternative approach that seems more promising was suggested by V.Visnjic /3/ and can be described as the macroparticle simulation using the discrete particles and the time-domain response functions of the pickup-kicker (PU-K) circuits. Since it is not possible to use the realistic number of \bar{p} that is about 10^{10} , one needs an appropriate scaling law to extrapolate from the results with a smaller number of particles. In this note, we present such a scaling law for an idealized momentum-cooling system (without coupling to transverse dynamics). In addition, another useful scaling law that allows to change the bandwidth is derived. An efficient macroparticle time dynamics algorithm is obtained, and some preliminary results of simulation are presented. The feasibility of macroparticle

*Operated by the Universities Research Association, Inc. under contract with the U.S.Dept. of Energy.

simulation is established by numerically testing the scaling laws. The full coupled simulation was not attempted yet and this remains to be done in the future.

2 Theory and algorithms.

2.1 Scaling laws for the Fokker-Planck model.

We base our discussion on the theoretical derivation of Ref./4/ (BL). The Fokker-Planck model of the evolution of momentum distribution function $\Psi(x, t)$ (with x for momentum deviation from the reference particle $x = E - E_0$ and t for time) is given by (BL50) as:

$$\frac{\partial \Psi}{\partial t} = -\frac{\partial}{\partial x} \left[F(x, t) \Psi - D(x, t) \frac{\partial \Psi}{\partial x} \right] \quad (1)$$

where the “damping” $F(x, t)$ and “diffusion” $D(x, t)$ are:

$$F(x, t) = \sum_l \frac{G_l(x)}{\epsilon_{-l}(x, t)} \quad (2)$$

$$D(x, t) = \Psi(x, t) \frac{N\pi}{\left| \frac{d\omega}{dx} \right|} \sum_l \frac{1}{|l|} \left| \frac{G_l(x)}{\epsilon_{-l}(x, t)} \right|^2 + D_{th}(x) \quad (3)$$

where $\omega(x)$ is the revolution frequency dependence on momentum, G_l and ϵ_l are respectively the gain and the signal suppression factor at harmonic l of the revolution frequency. The latter quantity is defined by:

$$\epsilon_{\pm|l|}(x, t) = 1 + \frac{N}{|l|} \int_{\eta \rightarrow 0+} dx_1 \frac{G_{\pm|l|}(x_1) \frac{\partial \Psi(x_1, t)}{\partial x_1}}{\eta \pm i(\omega(x) - \omega(x_1))} \quad (4)$$

where N is the total number of particles. The distribution function $\Psi(x, t)$ is normalized $\int dx \Psi(x, t) = 1$. The diffusion intensity $D_{th}(x)$ is caused by the thermal noise in the pick-ups and the electronic circuits and is given by:

$$D_{th}(x) = \pi \left(\frac{l\omega}{2\pi} \right)^2 \sum_l \frac{P(l\omega(x))}{\epsilon_{-l}(x)} \quad (5)$$

where $P(\Omega)$ is the noise power density. The gain harmonics $G_l(x)$ are defined as $G(l\omega(x), x)$ of the general gain function $G(\Omega, x)$. In the expression (4), the Palmer cooling technique is implied, since the gain G stands under the integration /4/.

The crucial issue for the possibility of the macroparticle simulation is the existence of the scaling laws for the Fokker-Planck equation (1) that would allow to reduce the total number of particles N . It is resolved positively by identifying the (scaling law) transformation:

$$N' = \frac{N}{k}$$

$$\begin{aligned}
G'_l(x) &= kG_l(x) \\
P'_l(x) &= kP_l(x) \\
t' &= \frac{t}{k}
\end{aligned}
\tag{6}$$

that leaves the FPE (1) invariant. It should be noted that the flux $J = F\Psi - D\frac{\partial\Psi}{\partial x}$ is invariant under the transformation (6) together with the “screening factors” ϵ_l . The meaning of the transformation (6) in terms of the cooling rate is that by decreasing (increasing) the number of particles by a factor k and simultaneous increasing (decreasing) of the gain by the same factor, the cooling rate is increased by the factor k . Notice here that the FPE invariance is a stronger property than the cooling time invariance, since the latter may change as the cooling progresses while the former can not.

The transformation (6) allows us to reduce the number of particles for simulation purposes to what is numerically practical. It is important to realize however that this is only true when one extra condition is met: the number of particles within a “sample” has to be large, i.e.:

$$\frac{N}{WT} \gg 1
\tag{7}$$

where W is the bandwidth of the cooling system and T is the revolution frequency. Indeed, the condition (7) guarantees the wide separation of the coherent and incoherent (cooling) time scales that justifies the truncation of the BBGKY hierarchy in order to derive the FPE /4/.

The necessity to satisfy the condition (7) makes one to look for some other scaling laws that would allow to reduce the bandwidth and push down the number of particles still further. Indeed, in the example of the Fermilab Accumulator Ring the bandwidth of the momentum stacking system extends up to ~ 4500 revolution frequencies, so one would still need about 20000 – 100000 particles to satisfy the condition (7). That can be too many for practical application, as we show in the next section.

The transformation of the required type that we propose to use is:

$$\begin{aligned}
G'_l(x) &= G_{Rl}(x) \\
\omega'(x) &= \omega_0 + R(\omega(x) - \omega_0) \\
P'_l(x) &= \frac{P_l(x)}{R} \\
t' &= Rt
\end{aligned}
\tag{8}$$

where ω_0 is the revolution frequency of the reference particle $\omega_0 = \omega(0)$, while the index Rl is understood as the integer part $[Rl]$. The transformation (8) is defined for any positive R both larger and smaller than unity. Unlike the situation with the transformation (6), the FPE will be invariant under the “bandwidth transformation” (8) only approximately and only when both the original and the transformed bandwidths are large, $WT \gg 1$, $WT/R \gg 1$. Indeed, one can easily see that the signal suppression factors are transformed

as $\epsilon'_l = \epsilon_{Rl}$. Moreover, if the gain harmonics G_l change slowly, as a function of l , from $l_{min} \sim 0.5WT$ to $l_{max} \sim WT$, the summation over l in the formulas (2) and (3) for the damping and diffusion intensities can be substituted by integration, producing:

$$F'(x) = \sum_l \frac{G_{Rl}}{\epsilon_{-Rl}} \approx \frac{1}{R} \sum_l \frac{G_l}{\epsilon_{-l}} = \frac{F(x)}{R} \quad (9)$$

and similarly $D'(x) = D(x)/R$. When $R > 1$, the transformation (8) reduces the bandwidth and the cooling slows down proportionately. Notice that the flux J is transformed as $J' = J/R$

Finally, one more transformation that rescales the gain without a change in the number of particles is:

$$\begin{aligned} G'_l(x) &= k_1 G_l(x) \\ \omega'(x) &= \omega_0 + k_1(\omega(x) - \omega_0) \\ P'_l(x) &= k_1 P_l(x) \\ t' &= \frac{t}{k_1} \end{aligned} \quad (10)$$

The flux J for this transformation scales as $J' = k_1 J$.

The three transformations (6), (8) and (10) allow to adjust independently three parameters, e.g. gain strength, bandwidth and frequency spread. All three transformations should be implemented to increase the speed of the macroparticle simulation, as is discussed in the following sections.

2.2 Dynamics with cooling: efficient algorithms.

The longitudinal equations of motion in a ring with one PU and one K can be defined as :

$$\begin{aligned} \dot{x}_i &= -q \delta_{2\pi}(\theta_i - \theta^K) \\ \dot{\theta}_i &= \omega(x_i) \\ \ddot{q} &= \sum_i H(x_i) \delta_{2\pi}(\theta_i - \theta^{PU}) + \int_0^\infty d\tau F(\tau) q(t - \tau) \end{aligned} \quad (11)$$

where x_i is the relative energy of the i -th particle $x_i = E_i - E^0$, θ_i is the azimuthal coordinate, and θ^K, θ^{PU} are the azimuthal locations of respectively the PU and the K. The quantity $q(t)$ is the voltage at the kicker as a function of time, the function $H(x)$ describes the position sensitivity of the PU in the Palmer cooling method /4/, and the retarding kernel $F(\tau)$ accounts for the net effect of amplifiers and filters. The time-domain dynamics (11) can be related to the more conventional frequency-domain calculations /4/ by using the fast-time (unperturbed) oscillations $\theta_i = \theta_{i0} + \omega(x_i)t$, yielding:

$$q(t) = \sum_{l=-\infty}^{\infty} \sum_i \frac{H(x_i) e^{il(\theta_{i0} + \omega(x_i)t - \theta^{PU})}}{\omega^2(x_i) - F_\omega(\omega(x_i))} \quad (12)$$

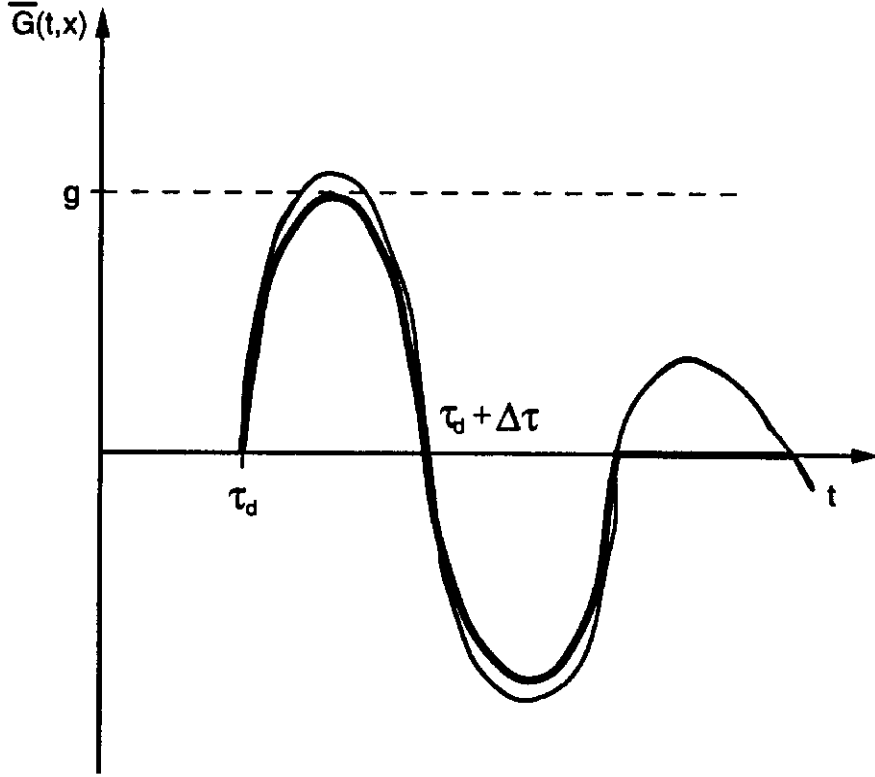


Figure 1: Typical time dependence of the Green function $\bar{G}(t, x)$ (lightcurve). Heavy curve is an “idealized” dependence that is used in the simulation code. Upper and lower “humps” on the dashed curve are parabolic.

where $F_\omega(\omega)$ is the Fourier image of $F(\tau)$. The gain $G(\Omega, x)$ is then:

$$G(\Omega, x) = \frac{H(x)e^{i(\theta^K - \theta^{PU})}}{\Omega^2 - F_\omega(\Omega)} \quad (13)$$

and $G_l(x) = G(l\omega(x), x)$. The form (13) can describe both the Palmer cooling when the denominator is nonzero at $\Omega = l\omega_0$ while $H(0) = 0$ and the filter cooling, when $H(0) \neq 0$ and $l^2\omega_0^2 = F_\omega(l\omega_0)$.

In time domain, the dynamical solution of the equation for q (11) can be presented as :

$$q(t) = \sum_{k=1}^{\infty} \sum_i \bar{G}(t - \tilde{t}_k^i, \tilde{x}_k^i) \quad (14)$$

where i is the particle number, \tilde{t}_k^i is the moment of crossing the PU number k (counted from moment t backwards), and \tilde{x}_k^i is the momentum x_i at that crossing. The Green function $\bar{G}(t, x)$ is the Fourier transform of the gain $G(\Omega, x)$.

The typical time dependence of the Green function $\bar{G}(t, x)$ is shown in Fig.1.

The Green function $\bar{G}(t, x)$ is zero for $\tau < \tau_d$, where τ_d is the PU-K delay time. The width of the impulse $\Delta\tau = \tau_{max} - \tau_d$ is determined by the bandwidth $W = 2\pi/\Delta\tau$. Though

for any real filter the “tail” of the Green function is nonzero at $t > \tau_{max}$, for the purpose of our macroparticle simulation we will consider an approximation of zero $\bar{G}(x, t)$ for $t > \tau_{max}$, substituting thus the real Green function by the one with the “tail cut-off”, as shown in Fig.1. This approximation allows one to have only a finite (and relatively small) number of particles that have crossed the PU to contribute to the K voltage at any given moment of time. More specifically, there will be only about $N_s \sim N\Delta\tau/T$ particles at their latest PU crossing moments of time $\tilde{t}_1^i = \tilde{t}^i$ that contribute to the sum (14).

Consider now the ways of casting the dynamics (11) in the form of mappings, with time advancing in discrete steps. A natural way of doing that would be to choose the discrete moments of time of the mapping to correspond to the successive crossings of the K by the particles. The (varying) time step therefore will be of the order T/N , and each particle receives a phase advance, though only one experiences the kick at the K. The number of computations per revolution therefore will be of the order of N^2 . This is a rather inefficient algorithm, and one would like to do better than that.

A more efficient algorithm can be constructed by devising a mapping in time steps of the order of the revolution period. More precisely, we suggest to take the time step equal to the minimal time-of-flight between the K and the PU. It can be estimated by taking the minimal (or maximal, if the sign of the momentum compaction factor α is negative) energy of the particles in the beam x_{min} , so that $\tau_0 = (\theta^K - \theta^{PU})/\omega_{min}$, $\omega_{min} = \omega(x_{min})$. Within that time step, the moments of time \tilde{t}^i and respective momenta \bar{x}^i of the particle arrival at the PU can be found from the initial phases and momenta (at the beginning of the time step) without the knowledge of the K voltage $q(t)$. That information, together with the same arrays stored in memory from the previous time step, directly defines the K voltage through the summation (14) at any given moment of time within the step. The general mapping for each particle from t_n to $t_{n+1} = t_n + \tau_0$ would consist then of the following stages:

- 1) Check if the particle crosses the PU. Compute and record crossing coordinates \tilde{t}^i if yes.
- 2) For each particle, check if it crosses the K within the time step. If not, apply “unperturbed” mapping, without a kick. Compute the K crossing time \tilde{t}^i if yes. Compute the K voltage $q(\tilde{t}^i)$ by using \tilde{t}^i and \bar{x}^i from this and previous step. Implement the kick and the unperturbed mapping from \tilde{t}^i to t_{n+1} .

Most of the computational resources in this algorithm are expended on the computations of the voltage $q(\tilde{t}^i)$, since each of these involves the summation over N_s particles in the sample. In order to identify these particles, we suggest to order the array of particle phases $\theta(i) = \theta_i$ once per time step and store the resulting array $\bar{\theta}(i)$. Since the revolution frequency spread is small, the relative ordering will not change much within a time step. That allows to single out the contributing particles by using the approximate homogeneous distribution in phases: $\bar{\theta}(i) \approx 2\pi i/N$. Indeed, the time coordinates of the PU crossing of the sample are $t_{min} = \tilde{t}^i - \tau_{max}$ and $t_{max} = \tilde{t}^i - \tau_d$. The azimuthal boundaries of the sample at $t = t_n$ can be found then, in case of $t_{min} > t_n$, as $\theta_{min} = \theta^{PU} - \omega_{max}(t_{max} - t_n)$,

$\theta_{max} = \theta^{PU} - \omega_{min}(t_{min} - t_n)$ (here $\omega_{min}, \omega_{max}$ are the smallest and the largest revolution frequencies in the beam). The particles in the sample are approximately those with i between $i_{min} = \theta_{min}N/2\pi$ and $i_{max} = \theta_{max}N/2\pi$. In practice, the sample has to be taken somewhat wider because of the statistical fluctuations in the particle positions. In case of $t_{min} < t_n$ one can similarly find the coordinates of the sample at the previous mapping step t_{n-1} and use arrays $\bar{\theta}, \bar{x}$ from the previous step to compute the voltage q .

The computational efficiency of this algorithm is about $N/N_s = 1/WT$ times better than that of the previous one. The time step depends on the K to P distance but is always of the order of the revolution period. The ordering procedure requires $\sim N \ln N$ operations per time step, but since there are $\sim N_s N$ operations to compute the voltage $q(t)$, the ordering does not significantly increase the total number of operations if $N_s \ll \ln N$. The estimate of the number of operations per revolution is $\sim N_s N$.

One can deduce now the computational benefit of the number of particles and bandwidth scaling transformations (6), (8) and (10). The relevant indicator is the number of operations N_{comp} per cooling time $\tau_c \sim TN_s/G/1/$, estimated thus as $N_{comp} \sim NN_s\tau_c$. The number-of-particles transformation (6) scales N and N_s as $N' = N/k, N'_s = N_s/k$, while the bandwidth transformation (8) scales N_s only as $N'_s = NR$. The frequency- spread transformation (10) scales the cooling time as $\tau'_c = \tau_c/k_1$. As a result, the number of operations per cooling time scales as $N'_{comp} = R^2 N_{comp}/k_1 k^3$. Since the parameter k_1 can not be increased significantly because of the Schottky band overlap condition, and also due to the condition (7) of the large number of particles per sample $N_s R/k \gg 1$, the best strategy to reduce the number of operations is to increase k (reduce the number of particles) while increasing R (reducing the bandwidth) to stay within the limits of that restriction. The only limitation to such procedure comes from a particular setup of our numerical algorithm that requires the sample to be much shorter than the circumference of the ring. One can expect thereby to be able to simulate an arbitrary number of particles, by as few as about a few thousand "macroparticles".

2.3 Schottky spectra.

One of the most important diagnostic tools in the real experimental environment are the Schottky signal monitors /1,5/. In order to be able to compare the simulation data with the experimental one, one needs to calculate the Schottky spectra in simulataion. The Schottky spectrum $S(\omega)$ can be calculated by using the definition:

$$S(\omega) = \lim_{T_s \rightarrow \infty} \int_0^{T_s} dt e^{i\omega t} K(t) \quad (15)$$

where the auto-correlation function $K(\tau)$ is defined as:

$$K(\tau) = \lim_{T_k \rightarrow \infty} \frac{1}{T_k} \int_0^{T_k} dt I(t)I(t + \tau) \quad (16)$$

The PU current $I(t)$ is the sum of the δ -functional impulses from each particle traversing the PU at $\theta = 0$:

$$I(t) = \sum_i \omega(x_i(t)) \delta(\theta_i(t)) \quad (17)$$

where $\delta(\theta)$ is the 2π -periodic delta-function and we assumed a momentum-insensitive PU. In simulation, the integrations in the formulas (15) and (16) are done in the finite ranges T_s and T_k . Within given computational resources, the ratio N/T_k and parameters T_k , T_s have to be chosen optimally in order to minimize the fluctuations of the Schottky spectra. Consider the no-cooling case, when the energies of the particles do not change. The (fluctuating) power spectrum $\tilde{S}(\omega)$ can be presented as:

$$\tilde{S}(\omega) = \omega_0^2 \sum_{i,j} \sum_m \sum_n f_m f_n \exp(i(m\theta_{i0} + n\theta_{j0})) \delta_{1/T_k}(m\omega_i + n\omega_j) \delta_{1/T_s}(\omega - m\omega_j) \quad (18)$$

where $\omega_i = \omega(x_i)$ and the small deviations of ω_i factor in front of δ functions were neglected by using $\omega_i = \omega_0$. The quantities f_m are the Fourier expansion coefficients of the periodic finite-width impulse from each particle $V_i(t) = f(\omega_i t + \theta_{i0}) = \sum_m f_m e^{im(\omega_i t + \theta_{i0})}$. The width of $f(\theta)$ is determined by the Schottky PU-analyzer bandwidth. That bandwidth $\omega_{max} = M\omega_0$ defines the maximal index M at which the summation in the expression (17) is effectively cut off. The function $\delta_{1/T}$ is the finite-width approximation of the delta function $\delta(\omega) = \lim_{T \rightarrow \infty} \delta_{1/T}(\omega)$ that is defined by:

$$\delta_{1/T}(\omega) = \frac{\exp(i\omega T) - 1}{i\omega} \quad (19)$$

The power spectrum \tilde{S} is the fluctuating quantity that depends on the random variables $\theta_{10} \dots \theta_{N0}$, $\omega_1 \dots \omega_N$. The average spectrum $S(\omega)$ over that ensemble, with a homogeneous distribution of θ_{i0} 's and distribution $\rho(\omega)$ of ω_i 's can be evaluated from the expression (18) to be:

$$S(\omega) = N^2 f_0^2 \omega_0^2 T_k \delta'_{1/T_s}(\omega) + N T_k \omega_0^2 \sum_{m \neq 0} |f_m|^2 I_m(\omega) \quad (20)$$

where $\delta'_{1/T}(\omega) = \text{Re}(\delta_{1/T}(\omega))$ and the function $I_m(\omega)$ is defined by:

$$I_m(\omega) = \int d\omega_1 \rho(\omega_1) \delta'_{1/T_s}(\omega - m\omega_1) \quad (21)$$

The function $I_m(\omega)$ equals to $\frac{1}{m} \rho(\frac{\omega}{m})$ when the integration time T_s is large enough $T_s > \frac{1}{m\delta\omega}$ and the frequency ω lies within a nonoverlapped Schottky band $|\omega - m\omega_0| \sim m\delta\omega$, $m\delta\omega \ll \omega_0$. Thus, the Schottky bands of the measured spectrum provide a direct observation of the frequency distribution $\rho(\omega)$.

Consider now the fluctuations of the power spectrum $\tilde{S}(\omega)$, described by the r.m.s. value:

$$P(\omega) = \langle (\tilde{S}(\omega) - S(\omega))^2 \rangle \quad (22)$$

where the average is over the variables $\theta_{10}\dots\theta_{N0}$ and $\omega_{10}\dots\omega_{N0}$. Substituting expressions (18) and (20) and carrying out the averages over $\theta_{10}\dots\theta_{N0}$ leaves the summation over only two indices m, n and i, j as the cross terms are averaged out. After some bulky manipulations and splitting the summation into the diagonal $i = j$ and nondiagonal $i \neq j$ parts one arrives to:

$$\begin{aligned}
P(\omega) = & \omega_0^4 \sum_{m \neq 0} \sum_{n \neq 0} |f_m|^2 |f_n|^2 \left[NT_k^2 \left(\int d\omega_1 \rho(\omega_1) \delta_{1/T_s}(\omega - m\omega_1) \delta_{1/T_s}(\omega - n\omega_1) \right. \right. \\
& - I_m(\omega) I_n(\omega) \left. \left. + N(N-1) \int d\omega_1 d\omega_2 \rho(\omega_1) \rho(\omega_2) \left| \delta_{1/T_k}(m\omega_1 + n\omega_2) \right|^2 \right. \right. \\
& \left. \left. \delta_{1/T_s}(\omega - m\omega_1) \left(\delta_{1/T_s}(\omega + m\omega_2) + \delta_{1/T_s}(\omega + n\omega_1) \right) \right) \right] \quad (23)
\end{aligned}$$

One can notice now that the terms with $m \neq n$ are suppressed by the factors $\omega_0/T_k, \omega_0/T_s$ that come from nonzero-argument functions $\delta_{1/T_k}, \delta_{1/T_s}$. Leaving only the leading terms, one obtains:

$$\begin{aligned}
P(\omega) = & \omega_0^4 \sum_{m \neq 0} |f_m|^4 \left[NT_k^2 \left(\int d\omega_1 \rho(\omega_1) \left| \delta_{1/T_s}(\omega - m\omega_1) \right|^2 - I_m^2(\omega) \right) + \right. \\
& \left. N(N-1) \int d\omega_1 d\omega_2 \rho(\omega_1) \rho(\omega_2) \left| \delta_{1/T_k}(m(\omega_1 - \omega_2)) \right|^2 \right. \\
& \left. \delta_{1/T_s}(\omega - m\omega_1) \delta_{1/T_s}(\omega - m\omega_2) \right] \quad (24)
\end{aligned}$$

Using the conditions $T_k \gg 1/\delta\omega, T_s \gg 1/\delta\omega$, one can calculate the integrals in (24) as the convolutions with δ -functions if the frequency ω lies within a nonoverlapped Schottky band, $|\omega - m\omega_0| \sim m\delta\omega, m\delta\omega \ll \omega_0$. The relative amplitude of the fluctuations $\Delta S_m^2(\omega) = P(\omega)/S^2(\omega)$ presents itself then as:

$$\Delta S_m^2(\omega) = \frac{mT_s}{N\rho(\omega/m)} + \frac{T_s}{T_k} \quad (25)$$

where again only the leading terms were retained. The result (25) indicates that in order to minimize fluctuations of the measured Schottky spectra, one should always choose the parameter T_s at the minimal level that is still compatible with the requirement to resolve the m -th Schottky band: $T_s \gg 1/m\delta\omega$. The averaging time T_k on the other hand should be chosen so as to make the two terms in (25) about equal: $T_k \sim N/m\delta\omega$.

3 Simulation code and preliminary results.

The code that implements the algorithm of the preceding section was written in Fortran. A number of diagnostic tools were built into it, with the outputs in the graphic form. In the code, the integration in the correlation function (16) was carried out by dividing the time in the current dependence $I(t)$ into steps of the duration $\delta t = T/N$ and ‘‘spreading out’’ the

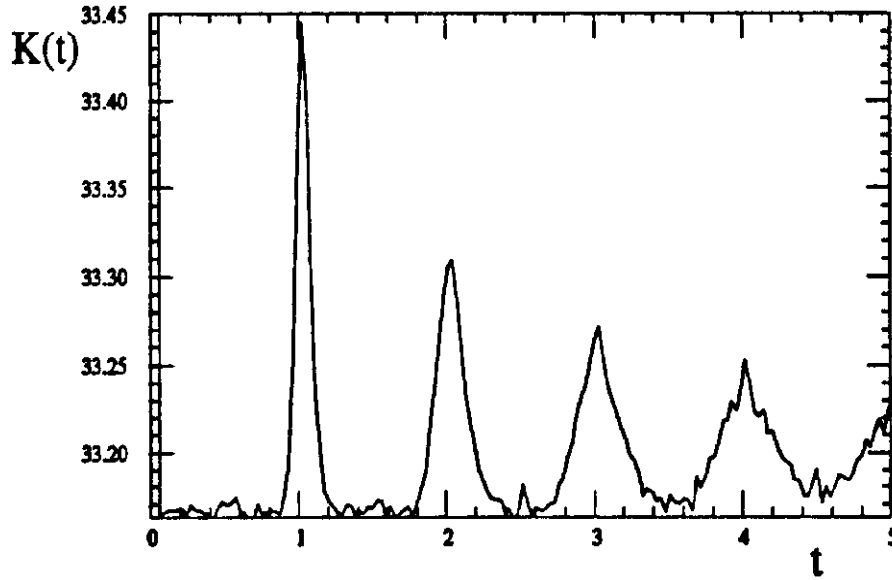


Figure 2: An example of the correlation function $K(\tau)$ for number of particles $N = 1000$, time step of the mapping $\tau_0 = .765$, nonlinearity $\lambda = .05$. Schottky computation parameters are $T_s = 50$, $T_k = 5000\tau_0$, $n_v = 30$.

delta-functional current impulses from each particle over n_v steps. The units of time are normalized so that $T = 1$. The cooling system is characterized by the gain g and the impulse width $\Delta\tau$ (inverse of the maximum passband frequency) as shown in Fig.1. In order to avoid the complications of the “bad mixing”, the section of the ring between the pickup and the kicker was considered to be isochronous, i.e. the parameter λ there was set to zero. The delay τ_d was matched so that the particle received the self-induced impulse at the kicker at the maximum of the first “hump” in Fig.1. The particles are distributed in momentum x initially in a Gaussian distribution with a unit r.m.s. size σ , while the revolution frequency depends on x as $\omega = 1 + \lambda x$. An example of the output of the correlation function $K(\tau)$ and the corresponding Schottky spectrum $\tilde{S}(\omega)$ for the case of no cooling is given in Figs.2 and 3.

An example of the cooling dynamics with parameters: number of particles $N = 1000$, impulse width $\Delta\tau = .05$, gain $g = .0002$ is shown in Figs.4,5,6 and 7. In Fig.4, the r.m.s. momentum spread $\sigma(t)$ is shown as a function of time t , measured in number of time steps. The time step of the mapping in this case is $\tau_0 = .5$. By the end of the cooling period $T_k = 10000\tau_0$ the momentum spread σ is diminished by about 5 times. That large decrease indicates that the gain g is much smaller than it’s optimal value (that would provide the fastest cooling). Indeed, for the optimal gain the “suppression factors” ϵ_l equal to 2. /1,4/ for each band l , so that the momentum spread is not far from the critical value of instability threshold and no big decrease in momentum spread without crossing the threshold is possible. In Fig.5, the time series of the momentum density profile are

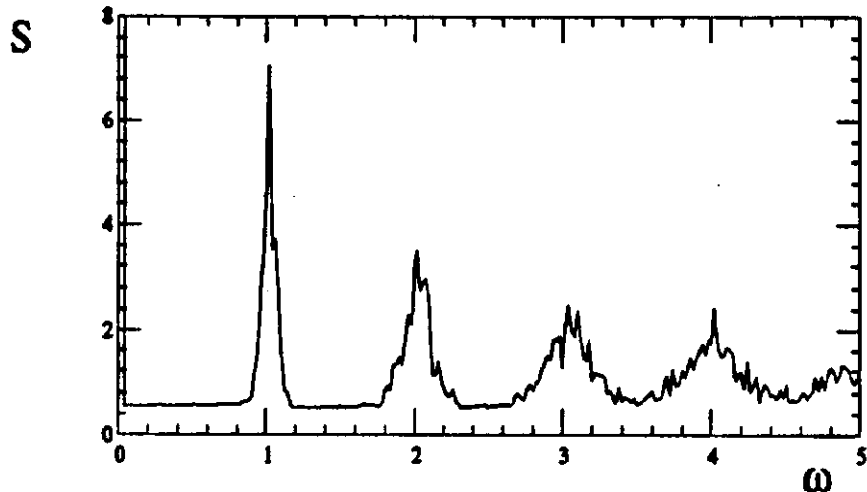


Figure 3: Power spectrum $S(\omega)$ for the case of Fig.2

presented. Ten equidistant in time snapshots (labelled sequentially) along the duration of the process are presented. The narrowing of the profiles together with a change of their shape (from Gaussian to triangle-like with practically no “tails”) in the course of cooling is clearly visible. In Fig.6 we present the same time series of the Schottky spectra $S(\omega)$ averaged over the time between the neighbouring “snapshots”. Again, the rise of the peaks because of the decrease of the momentum spread is clearly visible. In Fig.7, an averaged Schottky spectrum, with T_k equal to the total simulation time $10000\tau_0$ is presented. This Schottky spectrum is the average of the time series of Fig.6.

Two control runs to test the validity of the scaling laws (6) and (8) were made. First, the particle number scaling (6) was tested by simulating the example with 2.5 -times less particles ($N = 400$) and 2.5 -times higher gain ($g = .0005$) than in the example of Fig.4, all other parameters being the same. When the run time T_k was set at 2.5 times smaller value $T_k = 4000\tau_0$, the curve of the momentum spread versus time $\sigma(t)$ was undistinguishable from the one in Fig.4. The validity of the scaling law (6) tested out thereby perfectly well.

The second test was directed toward the “bandwidth” transformation (8). The impulse width $\Delta\tau$ and the nonlinearity λ were both reduced from the example of Fig.4 by 2.5 times to the values $\Delta\tau = .04$, $\lambda = .02$, while the gain g was increased by a factor 2.5 to the value $g = .0005$. When the run time T_k was set at 2.5 times smaller value than in the example of Fig.4, the curve of the momentum spread versus time $\sigma(t)$ was within a few percent deviation from the curve of Fig.4. The validity of the scaling law (8) tested out thereby as well as one could expect it to.

It should be noted here that since the momentum spread is cooled so much over the run of Fig.4, the test of scaling by comparing the curves $\sigma(t)$ with that of Fig.4 is very convincing, as the cooling rates for different momentum spread values are compared simultaneously.

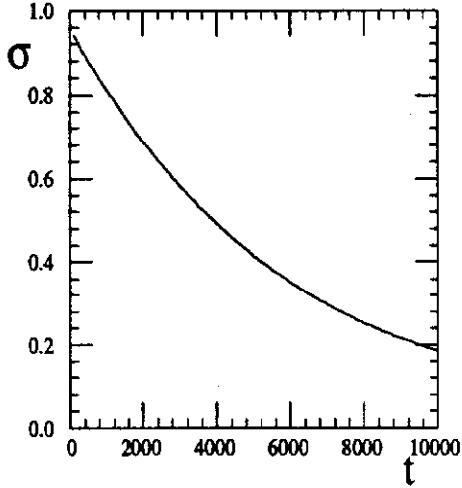


Figure 4: Momentum spread σ as a function of time t . Cooling system parameters are $\Delta\tau = .05$, gain $g = .0002$, number of particles $N = 1000$, nonlinearity $\lambda = .05$.

4 Momentum stacking.

The scaling laws of Section 1 can be implemented to simulate the momentum stacking of antiprotons. Consider the example of Fermilab Accumulator with the parameters:

$$\Delta N = 7 \cdot 10^7 \text{ (number of particles per injection)}$$

$$\Delta t = 2.4 \text{ sec (injection period)}$$

$$f_0 = 0.6 \text{ MHz (revolution frequency)}$$

$$f_{max} = 2 \text{ GHz, } f_{min} = 1 \text{ GHz (maximum and minimum frequencies of the stack-tail system passband)}$$

$$\Delta f = 135 \text{ Hz (revolution frequency spread of the stack)}$$

$$t_{max} = 40 \text{ Hrs (maximum stacking time)}$$

All three transformations (6), (8) and (10) have to be used in order to maximally reduce the number of particles and speed up the simulation. The limiting factors in this approach are the implicit assumptions in the derivation of the FPE (1). The first of these is the many-particle-per-sample" condition (7). The second one is the absence of the Schottky-band overlap in the rescaled system:

$$\frac{f'_{max}}{f_0} \frac{\Delta f'}{f_0} < 1 \tag{26}$$

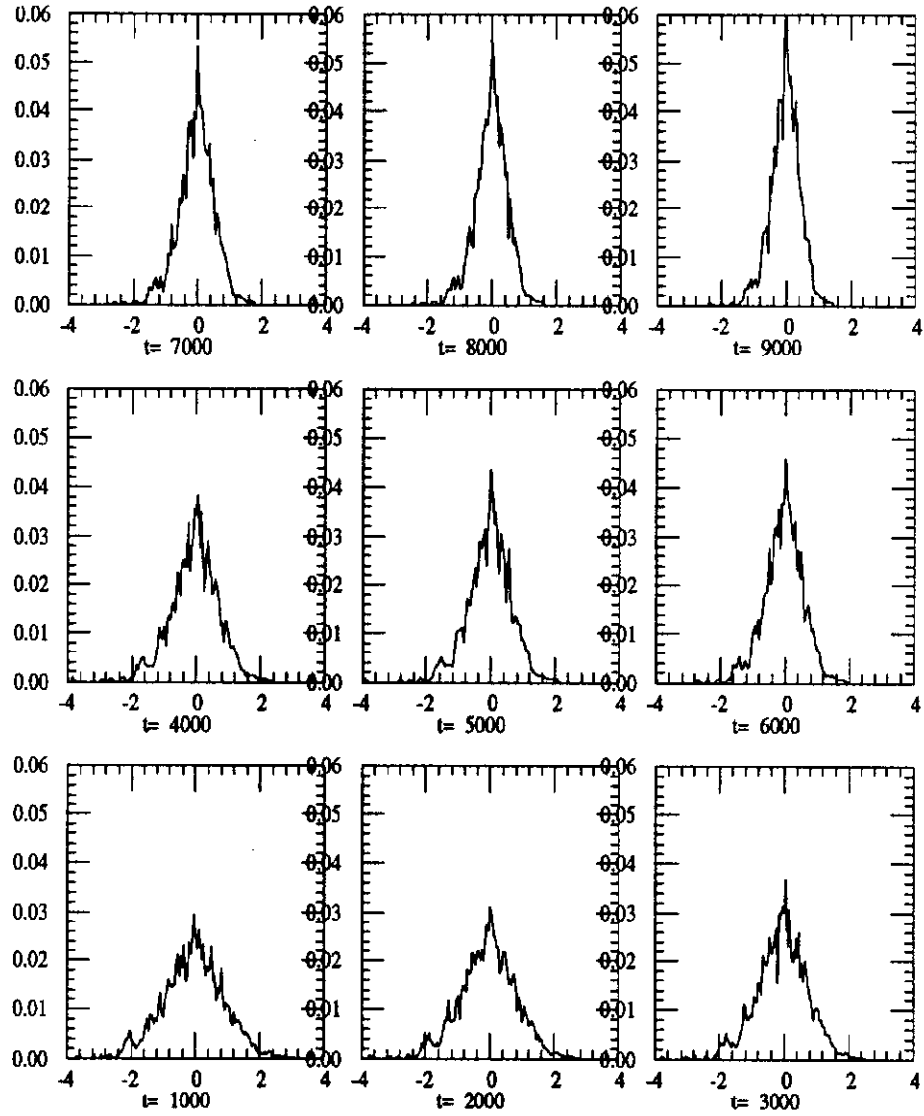


Figure 5: Momentum density profile evolution series for the case of Fig.4. Horizontal axis is momentum x ; snapshots are labelled by the time step number.

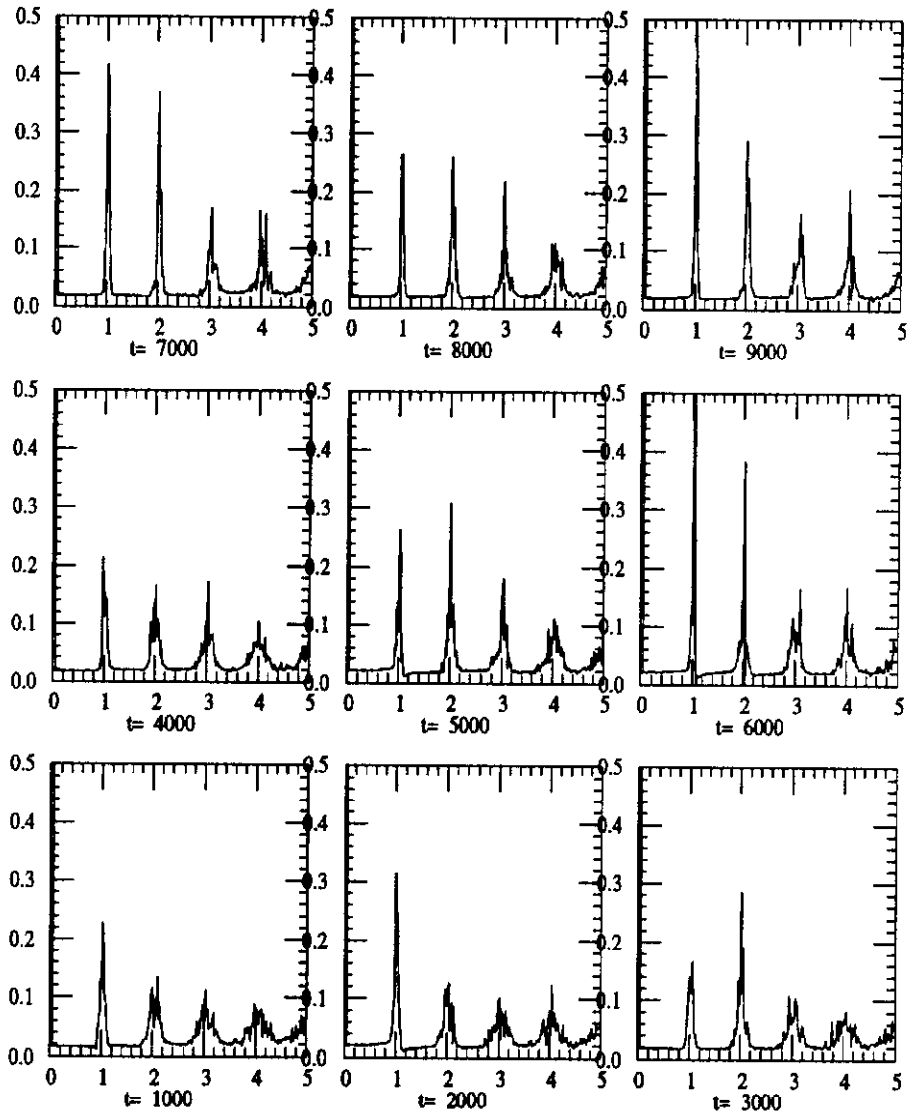


Figure 6: Power spectra evolution series for the case of Fig.4. Horizontal axis the frequency ω ; snapshots are labelled by the time step number.

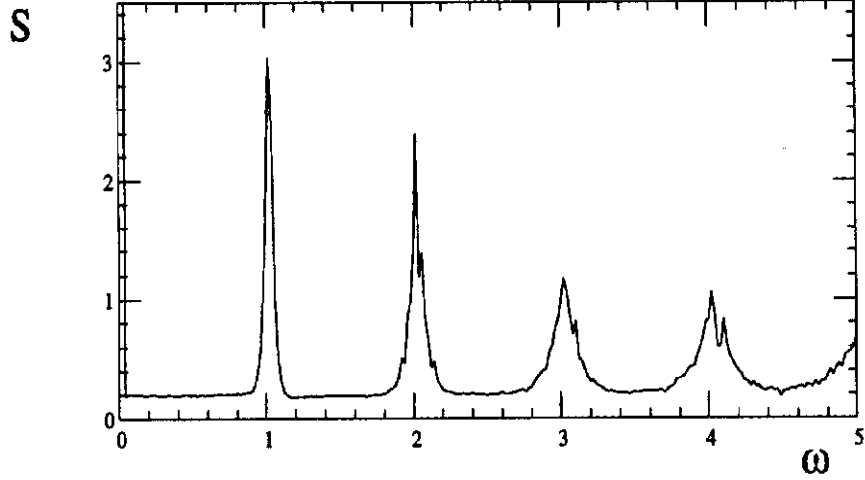


Figure 7: Average Schottky spectrum for the case of Fig.4.

Of all three transformations, only the transformation (10) changes the ratio $f'_{max}\Delta f'/f_0^2$. Consequently, for the case of Fermilab Accumulator, where that ratio is already close to unity, the scaling parameter k_1 in the transformation (10) can not be made larger than unity.

The third condition for the applicability of the FPE is the smallness of the “decoherence time” $\tau_d = 1/\lambda\sigma_x$ relative to the “cooling time” $\tau_c = \sigma/F(x)$:

$$\frac{\sigma_x}{F(x)} \gg \frac{E_0}{\eta\sigma_x} \quad (27)$$

where σ_x is the e-folding distance (in momentum) of the gain profile, η is the momentum compaction factor $\eta = (\delta f/f)/(\delta p/p)$, E_0 is the injection momentum and $F(x)$ is the “cooling force” (3). The condition (27) is most restrictive near the injection energy since the “cooling force” is maximal in that region. The maximum scaling constant k in the scaling transformation (6) is limited by the condition (27).

The transformations (8) and (10) are applied now by choosing the scaling parameters k_1 and R so as to increase the revolution frequency spread Δf and decrease the bandwidth $W = f_{max} - f_{min}$ to numerically convenient values. We choose the new maximum frequency f'_{max} from the condition $f'_{max}/f_0 = W/Rf_0 = 10$. The parameter R is found then to be $R = 330$. The parameter k_1 is chosen on the basis of a preference for a new injection current $J' = \Delta N'/\Delta t'$ of the magnitude:

$$J' = \frac{\Delta N}{f_0\Delta t} \frac{k_1}{R} = 0.1(\text{particles/turn}) \quad (28)$$

This value is deemed optimal in order to have a suitably long tracking time $T_{tr} \approx 5000 - 20000$ turns that would accommodate about 2.5 orders of magnitude of density variation over the stack tail. The parameter k_1 is found then to be $k_1 = .6$ and the rescaled frequency spread becomes $\Delta f'/f_0 = Rk_1\Delta f/f_0 = 0.05$.

The transformation (6) is applied by increasing the gain while keeping both parameters ΔN , Δt and therefore the injection flux constant. That speeds up the evolution of the distribution function $\rho'(x, t) = \rho(x, kt)/k$ (here the distribution ρ is not normalized $\rho = \Psi N(t)$, $\int \rho dx = N(t)$). The limiting factor to increasing the gain is the condition (27).

For the purpose of the proof-of-principle simulation a simplified model of the stacking system is used, with the purely exponential “pickup sensitivity” dependence $H(x) = H_0 \exp(x/\sigma_x)$ in the range of the dimensionless momentum variable from $x = 0$ (injection) to $x = -10$. For values of x smaller than -10 , the sensitivity is a linear function of momentum: $H = H_0(x - x_c)/(-10 - x_c) \exp(-10/\sigma_x)$ (x_c is less than -10). That region models the core system, and the core location $x = x_c$ is defined by the condition $H(x) = 0$. The Green function time dependence $\tilde{G}(t)$ is shown in Fig.8. Notice that the integral of the Green function over time has to be zero, since the gain is zero at zero frequency.

Two examples of stacking simulation results are shown in Figs.8 and 9. The width $\Delta\tau$ of the Green function impulses is $\Delta\tau = 0.05$, which approximately corresponds to the maximum passband frequency $f_{max}/f_0 = 10$. Other parameters are: frequency spread $\Delta f/f_0 = 0.05$, core position $x_c = -10.2$, pickup sensitivity e-folding distance $\sigma_x = 2.1$, injection period $\Delta t = 20$ (turns), injection number of particles $\Delta N = 2$. The plotted graphs are ten successive (equidistant in time) profiles of the base 10 logarithm of the density distribution. In order to improve the statistics of the density representation, each histogram comprises all particles at all time steps within the one-tenth of the total tracking time.

One can see that in the exponential region of the pickup sensitivity $H(x) = H_0 \exp(x/\sigma_x)$ the profiles approach the stationary distribution $\Psi \sim \exp(-x/\sigma_x)$ in accordance with an analytical solution of the FPE that is allowed in this region [1]. Overall, the profiles qualitatively resemble the ones that were obtained for the Accumulator by means of the Van der Meer simulation code, based on the FPE (see, e.g./1/), with about 2 orders of magnitude of density variations in the “tail” part and about one order of magnitude still more in the density variation in the “core” region. The most important conclusion overall is that we are able to reproduce 3 orders of magnitude of the dynamic range of variation of density.

An illustration of the distortions in the density profiles that start emerging when the gain is pushed too high is given in Fig.9. All parameters are the same as in the case of Fig.8, except for the twice larger gain $H_0 = 0.2$ and twice shorter tracking time $T_{tr} = 12000$ (turns) (so that the profiles should stay invariant if all restrictions (7), (26) and (27) are satisfied). One can notice some differences in the profiles of density even in the region not so close to the injection.

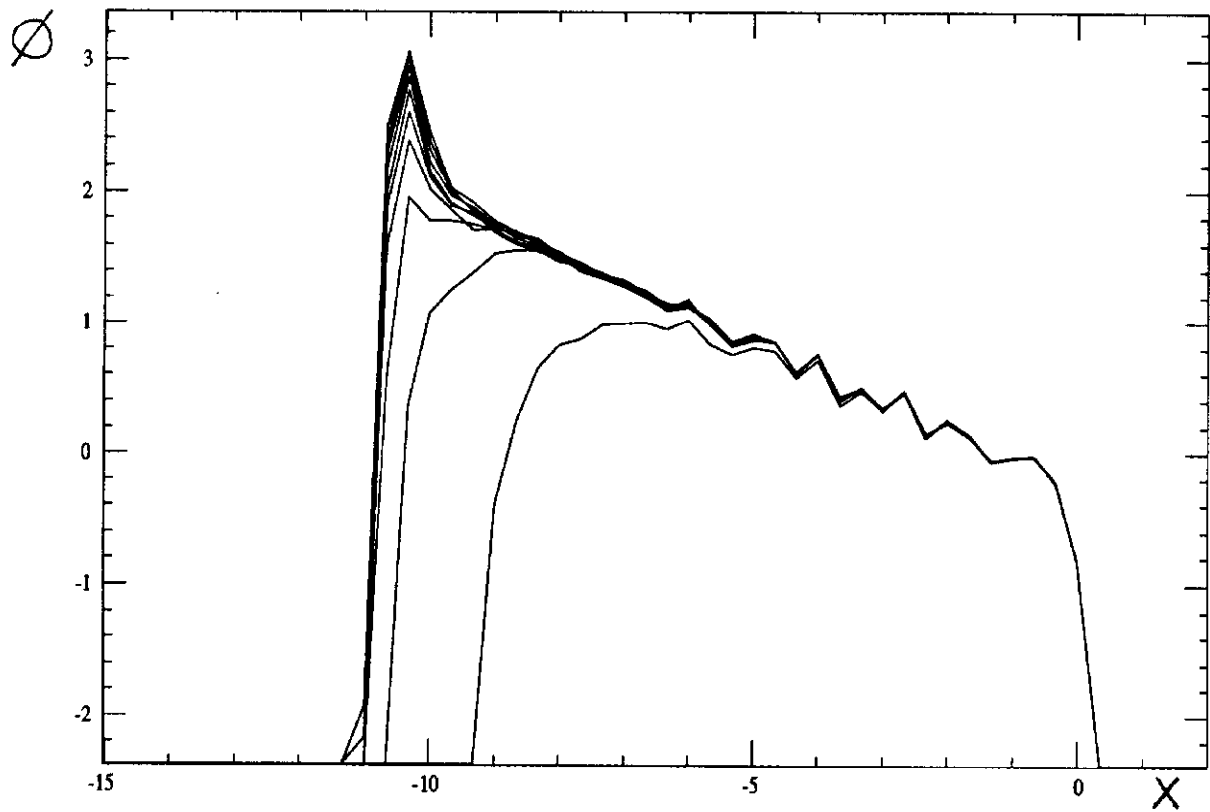


Figure 8: 10 Equidistant (in time) logarithmic density $\phi = \log_{10} \rho$ profiles. Tracking time $T_{tr} = 24000$ (turns). Gain strength is defined by $H_0 = 0.1$.

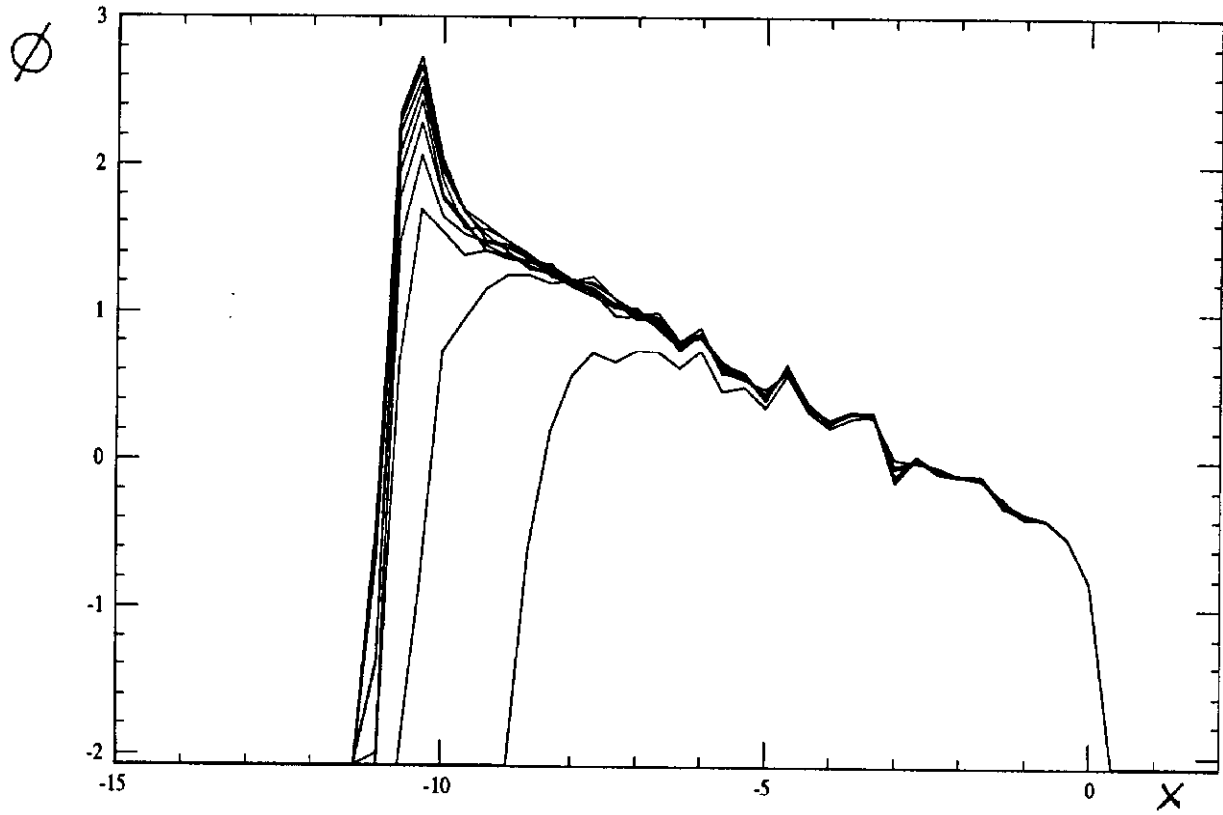


Figure 9: 10 Equidistant (in time) logarithmic density $\phi = \log_{10} \rho$ profiles for the parameters of Fig.8, but with a twice higher gain. Tracking time $T_{tr} = 12000$ (turns). Gain strength is defined by $H_0 = 0.2$.

5 Acknowledgements.

I wish to thank V.Visnjic and R.Pasquinelli for a number of useful discussions. The advice of M.Church on the specifics of cooling techniques and the final form and content of the paper was extremely helpful and is gratefully acknowledged.

References

1. A.V.Tollestrup, G.Dugan, Elementary stochastic cooling, Proc. 1981 SLAC Summer School on Accelerator Physics.
2. V.Visnjic, J.Marriner, "Van der Meer Cooling Simulation Code Manual", Fermilab, 1992 (unpublished).
3. V.Visnjic, private communication.
4. J.Bisognano, C.Leeman, Stochastic cooling, AIP Conf.Proc. N.87, Fermilab Summer School on Accelerator Physics, 1981.
5. M.Church, J.Marriner, Annu.Rev.Nucl.Part.Sci. 43 (1993) 253.